Band-Gap and Band-Edge Engineering of Multicomponent Garnet Scintillators from First Principles

Satyesh K. Yadav* and Blas P. Uberuaga
Materials Science and Technology Division, Los Alamos National Laboratory, Los Alamos, New Mexico 87545, USA

Martin Nikl
Institute of Physics, Academy of Sciences of the Czech Republic, 16253 Prague, Czech Republic

Chao Jiang
Thermo-Calc Software Inc., Pittsburgh, Pennsylvania 15317, USA

Christopher R. Stanek
Materials Science and Technology Division, Los Alamos National Laboratory, Los Alamos, New Mexico 87545, USA

(Received 11 April 2015; revised manuscript received 18 September 2015; published 24 November 2015)

Complex doping schemes in $R_3Al_5O_{12}$ (where R is the rare-earth element) garnet compounds have recently led to pronounced improvements in scintillator performance. Specifically, by admixing lutetium and yttrium aluminate garnets with gallium and gadolinium, the band gap is altered in a manner that facilitates the removal of deleterious electron trapping associated with cation antisite defects. Here, we expand upon this initial work to systematically investigate the effect of substitutional admixing on the energy levels of band edges. Density-functional theory and hybrid density-functional theory (HDFT) are used to survey potential admixing candidates that modify either the conduction-band minimum (CBM) or valence-band maximum (VBM). We consider two sets of compositions based on $Lu_3B_5O_{12}$ where B is Al, Ga, In, As, and Sb, and $R_3Al_5O_{12}$, where R is Lu, Gd, Dy, and Er. We find that admixing with various R cations does not appreciably affect the band gap or band edges. In contrast, substituting Al with cations of dissimilar ionic radii has a profound impact on the band structure. We further show that certain dopants can be used to selectively modify only the CBM or the VBM. Specifically, Ga and In decrease the band gap by lowering the CBM, while As and Sb decrease the band gap by raising the VBM, the relative change in band gap is quantitatively validated by HDFT. These results demonstrate a powerful approach to quickly screen the impact of dopants on the electronic structure of scintillator compounds, identifying those dopants which alter the band edges in very specific ways to eliminate both electron and hole traps responsible for performance limitations. This approach should be broadly applicable for the optimization of electronic and optical performance for a wide range of compounds by tuning the VBM and CBM.

DOI: 10.1103/PhysRevApplied.4.054012

I. INTRODUCTION

$A_3B_5O_{12}$ garnets and, in particular, $R_3Al_5O_{12}$ compositions (where R is rare-earth element or Y), have been studied for technical use as optical materials for over 50 years [1–3]. Although garnets also received interest as a scintillator approximately 20 years ago [4], a lower light yield than other compounds ultimately led to relative disinterest. Often, defects trap charge carriers, otherwise available to participate in the scintillation process, thus, potentially resulting in delayed and/or reduced light output. The important role that defects play in scintillator performance has been well documented [5]. However, recent studies involving codoping of garnets demonstrate dramatic improvements in light yield, and these findings, consequently, reinvigorate interest in garnets as high-performance scintillators [6–16]. These optimization efforts rely on the manipulation of the garnet electronic structure through admixing and in the process creating so-called "multicomponent" garnets [17]. It is well known that cation antisite defects are present in garnets (R^{3+} on Al^{3+} sites and vice versa) [18–23], and they contribute to reduced scintillator performance [24] by creating traps for the electronic carriers which results in considerable slowing down of scintillation response. However, the challenge of removing cation antisite defects in garnet is that they are isovalent (i.e., charge neutral), and the corresponding defect formation energy is rather low, thereby preventing a defect engineering approach.

*syadav@lanl.gov
yadav.satyesh@gmail.com

 © 2015 American Physical Society

Therefore, alternative defect management methods are required. Interestingly, it has been shown previously in the literature that adding Ga to aluminate garnets removes the signature of antisite defects [25]. This implies that Ga admixing eliminates the effectiveness of the antisite traps. However, Ga is closer in size to the *R* cation than it is to Al [26], which suggests that a higher concentration of antisites should exist in Ga-doped garnets than in pure aluminate garnets—a hypothesis validated by a joint experimental atomistic simulation study [27,28]. Rather, instead of reducing the concentration of deleterious antisite defects, the benefit of Ga admixing arises from shifts in the conduction band such that it envelops the trap state in the forbidden gap associated with the antisite defect [17,29]. This is a primary example of the "band-gap engineering" approach to defect management.

In this paper, we build upon our previous effort to optimize the electronic structure of multicomponent garnets by studying a range of dopants and their effect on the energy levels of band edges of $Lu_3Al_5O_{12}$. Our approach relies on manipulation of the electronic structure of a scintillator compound through doping in order to remove the deleterious effect of defects that may act as electron or hole traps. A key aspect of this approach is that the band edges must be shifted to envelop the shallow trap states, without also interfering with the activator transition. A simplified schematic showing the position of activator transition levels (with no splitting for illustration purposes) and electron and hole traps with respect to the valence and conduction bands is presented in Fig. 1. Band edges can be modified by doping to shift the valence and conduction bands. The level of band edges modified due to doping should eliminate only the defect states but should not lower the conduction-band minimum (CBM) or raise the valence-band maximum (VBM) to an extent that the Ce^{3+} transition levels fall in the conduction or valence bands. By using density-functional-theory (DFT)-based first-principles calculations, we show that certain 3+ dopants that substitute for Al can result in variations in either the valence- or conduction-band edges, while leaving the other band edge more or less unchanged, thus, opening the path for band-edge engineering through admixing. We also show that substituting Lu with *R* cations does not have a significant impact on band edges. Although we use garnet as a case study, it is anticipated that this approach can be extended to a wide range of scintillator compounds and provide an efficient manner to screen dopants for optimizing performance.

II. METHODOLOGY

A. First-principles method

DFT calculations are performed using the Vienna *ab initio* simulation package (VASP) [30]. The DFT calculations employ the Perdew, Burke, and Ernzerhof (PBE) [31] generalized-gradient approximation exchange-correlation functional and the projector-augmented-wave method [32]. The hybrid DFT calculations utilize the specific functional referred to as the HSE06 functional in the literature [33]. This functional is created by starting with the PBE exchange-correlation functional and replacing 25% of the PBE exchange interaction by a screened nonlocal functional with an inverse screening length of 0.2 $Å^{-1}$. For all calculations, a plane-wave cutoff of 500 eV for the plane-wave expansion of the wave functions is used to obtain highly accurate forces. In the results reported, only the gamma point is considered in the *k*-space sampling; however, we employ denser *k*-point meshes in select cases and very similar results are obtained. All structures are fully relaxed without any symmetry constraints, and relaxations are considered converged when each component of the force on every atom is smaller than 0.02 eV/Å.

B. Band-edge alignment

The first step to reliably determine the relative position of band edges in a compound as a function of composition is to identify a reference state that does not change with chemical

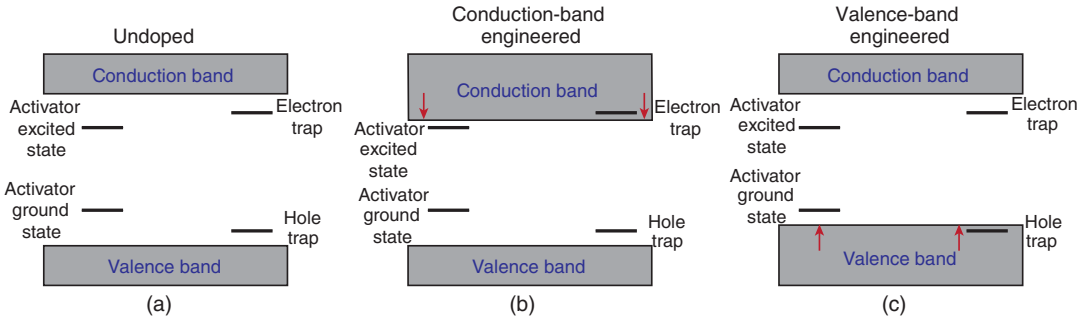

FIG. 1. A simplified schematic showing activator transition levels and electron and hole traps with respect to valence- and conduction-band edges of a scintillator, where (a) is the case of an undoped scintillator, where both electron and hole traps reside within the band gap, (b) illustrates the idealized scenario of the same scintillator that is strategically doped to shift only the conduction-band edge in order to envelop the electron trap (but not the excited state of the activator), and (c) shows the analogue case for the scintillator doped to modify the valence-band edge in order to envelop the hole trap (but not the activator ground state). Specific shifting of band edges is what is referred to as band-edge engineering.

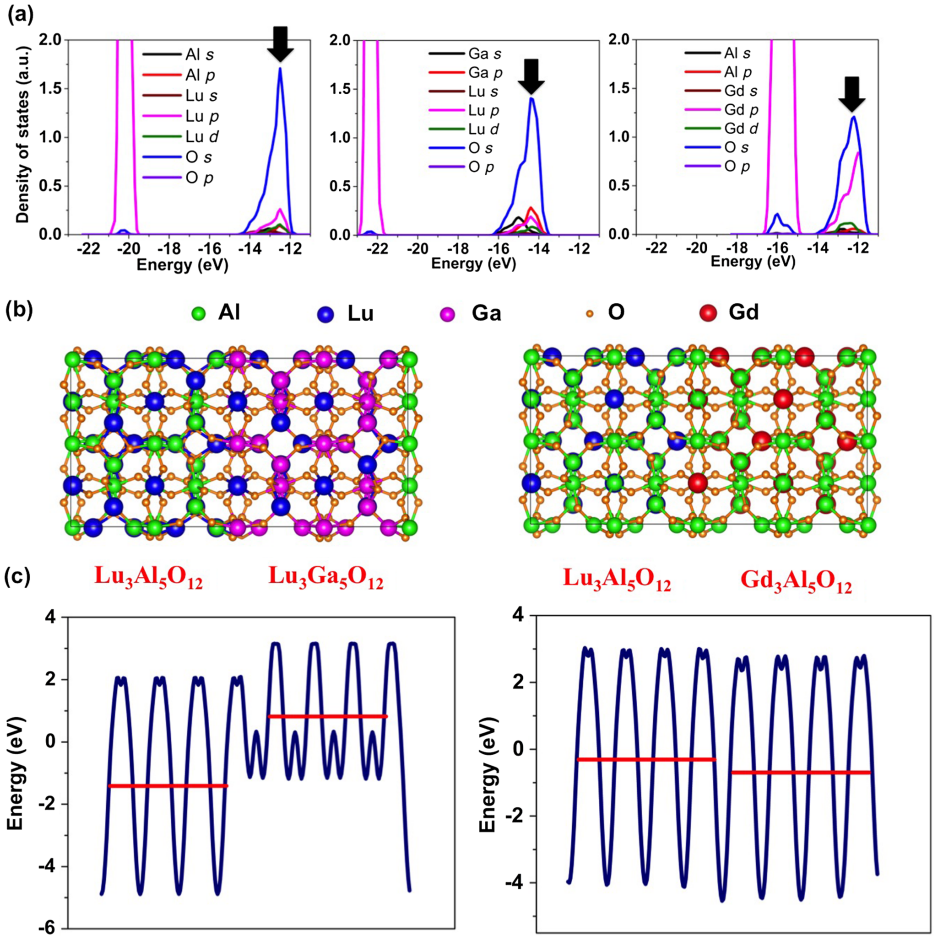

FIG. 2. (a) Density of states of deep states of $Lu_3Al_5O_{12}$, $Lu_3Ga_5O_{12}$, and $Gd_3Al_5O_{12}$, where the oxygen state that is used as a reference is marked by an arrow. (b) Supercell used for calculating electrostatic potentials, where Lu is blue, Al green, Ga magenta, O orange, Gd red. (c) Electrostatic potential calculated using the supercell in (b), where the red horizontal line indicates the average electrostatic potential.

composition. There are several references that are used in the literature to determine the relative position of band edges [34–37]. The average electrostatic potential is the best common reference, but it is very expensive to calculate as both materials of interest must be contained within one common simulation cell. Not only does this method necessitate large cells to accommodate both materials but also to avoid interfacial effects that are not of interest here. Rather than rely on a computationally intensive electrostatic potential approach, in this work we use a deep 2*s* state of oxygen as a reference to realign band edges of two compounds [34].

Figure 2(a) shows the density of states (DOS) plot of $Lu_3Al_5O_{12}$, $Lu_3Ga_5O_{12}$, and $Lu_3Gd_5O_{12}$, and the *s* state chosen for comparison is indicated by an arrow. It can be seen in Fig. 2(a) that the deep state chosen is dominant compared to all other orbitals at that energy making it an ideal candidate for band alignment, as this state is insensitive to the local coordination of the atoms and, thus, should have the same energy regardless of environment. With this deep state identified, the band edges of the two systems then can be compared directly by shifting the band structure of one such that the energy of the deep state coincides with the same state in the other structure.

TABLE I. Relative shift of band edges in electron volts as calculated using a deep *s* state (deep state) and aligning the electrostatic potential (electrostatic).

Method	$Lu_3Ga_5O_{12}$	$Gd_3Al_5O_{12}$
Deep state	1.9	0.4
Electrostatic	2.1	0.6

To validate the approach of employing the computationally less-intensive deep-state approach, we compare the relative shift with the average electrostatic potential for two cases (Al substitution with Ga and Lu substitution with Gd). Figure 2(b) shows the supercell used for calculating the average electrostatic potential. The offset between the two systems is calculated using the average electrostatic potentials for $Lu_3Al_5O_{12}$ and $Lu_3Ga_5O_{12}$ and $Lu_3Al_5O_{12}$ and $Gd_3Al_5O_{12}$. Table I shows the good agreement between the two methods for calculating the band offset, providing confidence that the deep *s*-state approach gives physically meaningful values.

III. RESULTS

A. Al substitution

First, we consider the extreme case of full Al substitution with larger cations. Using the deep *s* state of oxygen as the

common reference, we calculate the relative position of band edges of various $Lu_3B_5O_{12}$ compounds, where B is Al, Ga, In, As, and Sb. Other garnets are less common than Al garnets, with only $Lu_3Ga_5O_{12}$ [38–40] and $Lu_3Sb_5O_{12}$ [41] reported in the literature. However, analyzing how other B cations impact the electronic structure may guide future doping and admixing strategies where full substitution may not be required. Figure 3(a) shows the relative position of the CBM and VBM, along with the lattice parameters, for each of the compounds considered. Figure 3(b) shows the change in the band gap as a function of the lattice parameter.

The experimental band gap of $Lu_3Al_5O_{12}$ is 7.5–8.0 eV [42], which is in reasonably good agreement with the hybrid density-functional-theory-calculated band gap of 6.9 eV. However, what is important to this study is the relative change of band-gap energy (rather than absolute value), and this is predicted well with PBE. That is, the change in the band gap as calculated with both methods is in very good agreement. We have shown this before for ZnX (X is O, S, Se, and Te) compounds under uniaxial strains with d electrons [43,44]. This work indicates that PBE accurately predicts band-edge shifts even for materials with correlated electrons.

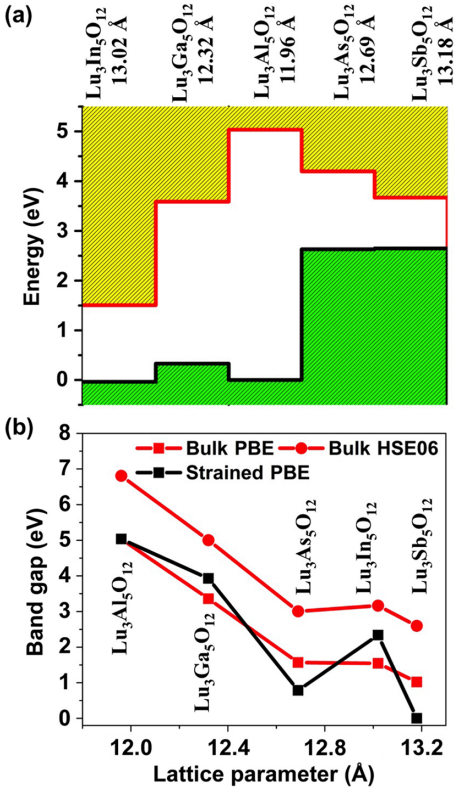

FIG. 3. (a) Conduction- and valence-band change for $Lu_3B_5O_{12}$ compounds, where B is Al, In, Ga, As, and Sb. (b) Change in band gap as a function of lattice parameter for the different compounds considered. The "bulk" (red) line indicates the band gap of the compound at its relaxed lattice constant (calculated using PBE and HSE06), while the "strained" (black) line is the band gap of the compound when placed at the lattice constant of $Lu_3Al_5O_{12}$ to better separate the roles of chemistry and strain on the changes in the band gap. The band gap for the strained compound is plotted versus the compound's natural lattice constant, for ease of comparison.

There are several observations that can be made from Fig. 3. First, $Lu_3Al_5O_{12}$ (LuAG) has the largest band gap of all compounds considered, and the band gap decreases with increasing lattice parameter. As has been observed previously, for $Lu_3Ga_5O_{12}$ (LGG), the CBM is shifted with respect to LuAG, while the VBM is only slightly shifted, and this shift in the CBM of LGG is related to the CBM shift observed in Ga-doped LuAG, which leads to the overlap of the cation antisite trap state [29]. A similar but more pronounced effect is observed for $Lu_3In_5O_{12}$, where the CBM is further shifted with respect to LuAG and LGG, but the VBM remains near to that of LuAG and LGG. Overall, while the VBM remains essentially constant when substituting Al with In and Ga, large CBM variations are observed. However, substituting Al with either As or Sb leads to significantly larger changes in the VBM while the associated shifts in the CBM are relatively modest; see Fig. 3. Thus, upon substitution of Al with As or Sb, the overall decrease in the band gap is primarily due to increased VBM energy. Although the VBM shifts observed for $Lu_3As_5O_{12}$ and $Lu_3Sb_5O_{12}$ are similar, the larger $Lu_3Sb_5O_{12}$ exhibits a larger CBM shift.

The difference between $Lu_3As_5O_{12}/Lu_3Sb_5O_{12}$ (i.e., large VBM shift) and $Lu_3In_5O_{12}/Lu_3Ga_5O_{12}$ (i.e., large CBM shift) can be understood by closely examining the states that constitute the CBM and VBM. For example, Fig. 4 shows the electronic DOS for $Lu_3Al_5O_{12}$, $Lu_3Ga_5O_{12}$, and $Lu_3In_5O_{12}$. The DOS of $Lu_3Al_5O_{12}$ shows that the CBM is comprised of a Lu d state, and the VBM is dominated by an O p state. In $Lu_3Ga_5O_{12}$ and $Lu_3In_5O_{12}$, the CBM shift is driven by Ga and In s states hybridizing with the O p state, which are, in these two cases, dominant contributors to the CBM. Figure 5 shows the DOS for $Lu_3Al_5O_{12}$, $Lu_3As_5O_{12}$, and $Lu_3Sb_5O_{12}$. In $Lu_3As_5O_{12}$ and $Lu_3Sb_5O_{12}$, the VBM shift is driven by As and Sb s states hybridizing with the O p state which are now dominant contributors to the VBM. This situation is similar to a shift of VBM in TiO_2 that is observed when S is substituted with O due to the strong hybridization of the S and O p states [45]. In addition to the prominent difference in hybridization of states in the two cases, Bader charge analysis shows that As and Sb bonds are more covalent compared to Ga and In bonds [46,47]. Thus, and as expected, more pronounced covalent bonding dopants such as As and Sb push the VBM higher in energy, while ionic (electronegative) bonding dopants such as Ga and In shift the CBM down in energy to reduce the overall band gap.

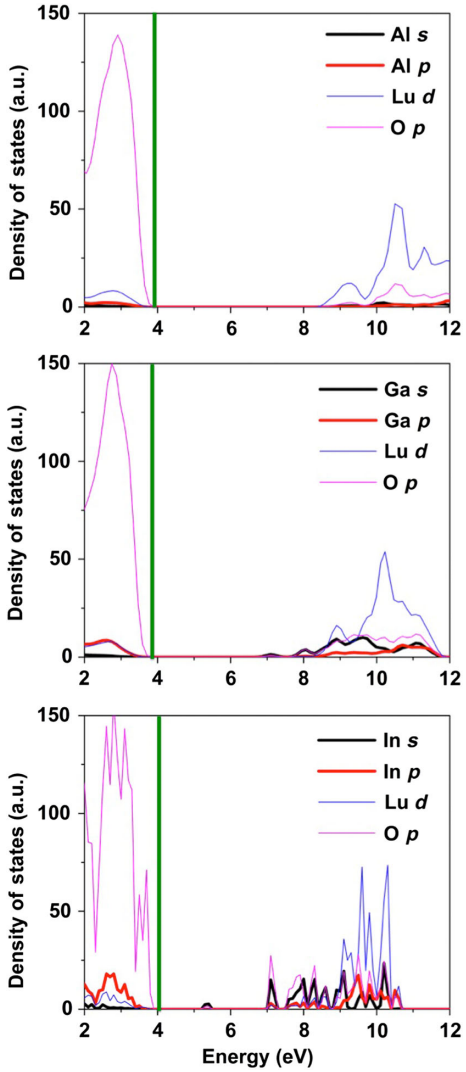

FIG. 4. Density of states arising from Al, Ga, and In s and p states, Lu d states, and O p states for garnets where B is Al, Ga, and In. The green vertical line corresponds to the Fermi level (highest occupied state) obtained by the alignment of the deep oxygen s state.

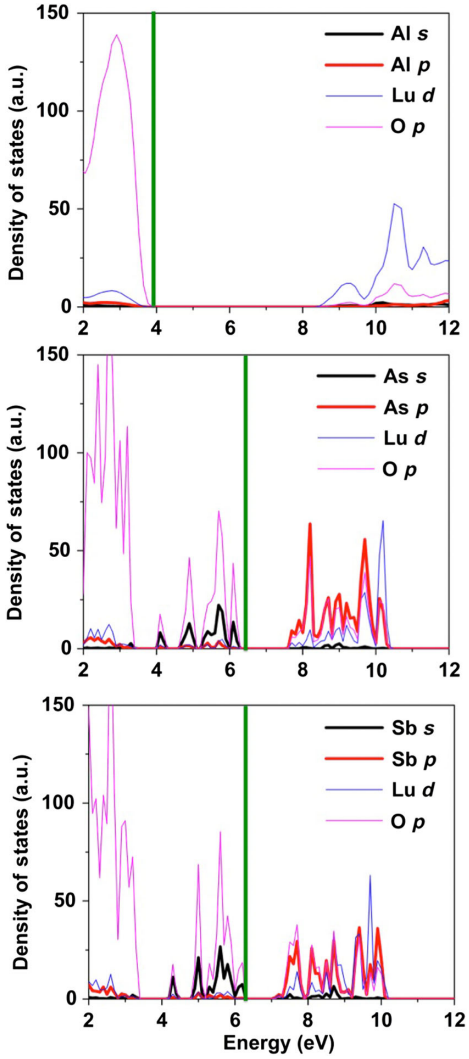

FIG. 5. Density of states arising from Al, As, and Sb s and p states, Lu d states, and O p states for garnets where B is Al, As, and Sb. The green vertical line corresponds to the Fermi level (highest occupied state) obtained by the alignment of the deep oxygen s state.

B. Electronic structure variation due to Lu substitution

Now we move to the extreme case of full Lu substitution with Gd, Dy, and Er to assess the effect of admixing on the R site on the band gap and band edges of LuAG. The relative position of the band edges of $R_3Al_5O_{12}$ (where R is Lu, Gd, Dy, and Er) is shown in Fig. 6(a). Figure 6(b) shows the change in the band gap as a function of the lattice parameter. Substituting Lu with Gd, Dy, or Er results in relatively small shifts in the band gap, which is commensurate with negligible variations in the lattice parameter. In all cases, the VBM and CBM shift in the same direction, resulting in an overall band gap that is relatively constant. It is also interesting to note that Lu, Gd, Dy, and Er $5d$ states dominate the bottom of the conduction band.

C. Effect of admixing concentration

Finally, we assess the role of the admixed species concentration on the band structure. That is, the above results consider only full substitution of Lu or Al cations in $Lu_3Al_5O_{12}$ rather than a partial replacement of Al or Lu, which is a more realistic scenario. Given that Gd and Ga are present in some of the multicomponent garnet compounds of interest for scintillating applications, we systematically assess how variations in their concentration modify the band-gap and band-edge position.

Figure 7(a) shows the variation in the band gap, Fig. 7(b) CBM, and Fig. 7(c) VBM as a function of Gd (x) and Ga (y) concentration in $(Lu_{1-x}Gd_x)_3(Al_{1-y}Ga_y)_5O_{12}$. The garnet structure contains one crystallographically unique Lu site but two crystallographically unique Al sites, of which 40% are octahedrally coordinated and 60% are

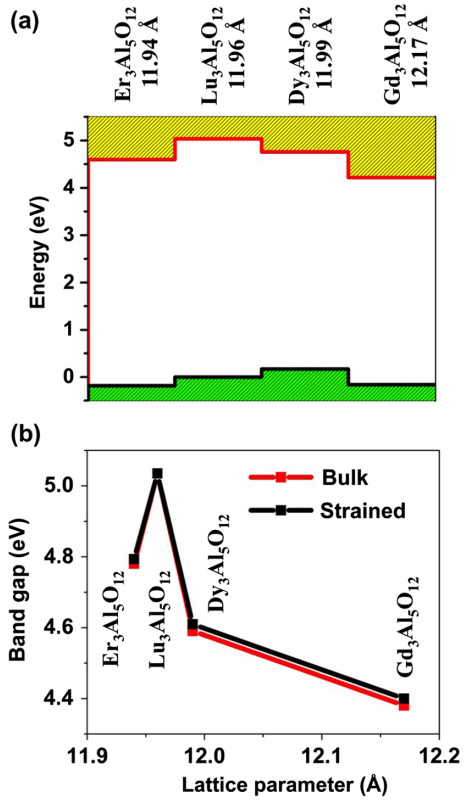

FIG. 6. (a) Conduction- and valence-band changes for $R_3Al_5O_{12}$ compounds, where R is Lu, Gd, Dy, and Er. (b) Change in the band gap as a function of the lattice parameter for the different compounds considered. The bulk (red) line indicates the band gap of the compound at its relaxed lattice constant, while the strained (black) line is the band gap of the compound when placed at the lattice constant of $Lu_3Al_5O_{12}$. The band gap for the strained compound is plotted versus the compound's natural lattice constant, for ease of comparison.

tetrahedrally coordinated. We use the special quasirandom structure (SQS) [48] approach to generate representative structures that mimic randomly substituted Ga and Gd amongst all of the sites. In generating the SQSs, we consider the tetrahedral and octahedral sublattices as distinct and construct SQSs in which the cations are distributed independently on these two sublattices. These SQSs are then combined to achieve the various levels of substitutional species. This leads to situations in which all of the substitutional species are on tetrahedral sites for one composition (e.g., 30%) and all on octahedral sites for the next composition (40%), leading to discontinuities in the properties between those compositions. However, the change in band gap depends more significantly on the total Ga content and less on the actual distribution between tetrahedral and octahedral sites.

It can be seen that the variation in band gap with Gd concentration is quite linear. The only deviation from linearity is observed when the position of the Ga switches from the octahedral to the tetrahedral site, as we discuss above. Ga present on tetrahedral sites leads to a larger reduction in the band gap and a larger CBM shift than when Ga is present on octahedral sites. Hence, there is an abrupt shift from 30% to 40% when Ga substitution transitions from all tetrahedral (at 30%) to all octahedral (at 40%) sites. In a truly random distribution of Ga, this abrupt shift will not occur, and the dependence on the band gap and CBM shift on the Ga concentration will be linear throughout the composition range. Furthermore, and as we discuss above for the cases of full substitution, the change in the band gap is much more sensitive to changes in the B cation than the A cation. Over most of the compositional range, the band gap is relatively insensitive to the Gd concentration, except for when the Ga content is very small. All of the change in the band gap in this compositional range is due to Ga-induced changes in the CBM.

The calculations of LuAG admixed with Ga suggest a linear relationship between band-edge shifts and Ga concentration. To verify the generality of linear band-gap variation as a function of Al substituent concentration in $Lu_3Al_5O_{12}$, we also calculate band-gap variations for In, As, and Sb substituting for Al as a function of admixed concentration; see Fig. 8. At small concentrations, In, As, and Sb have a more significant effect on the band-gap variation compared to Ga. An implication of this result is

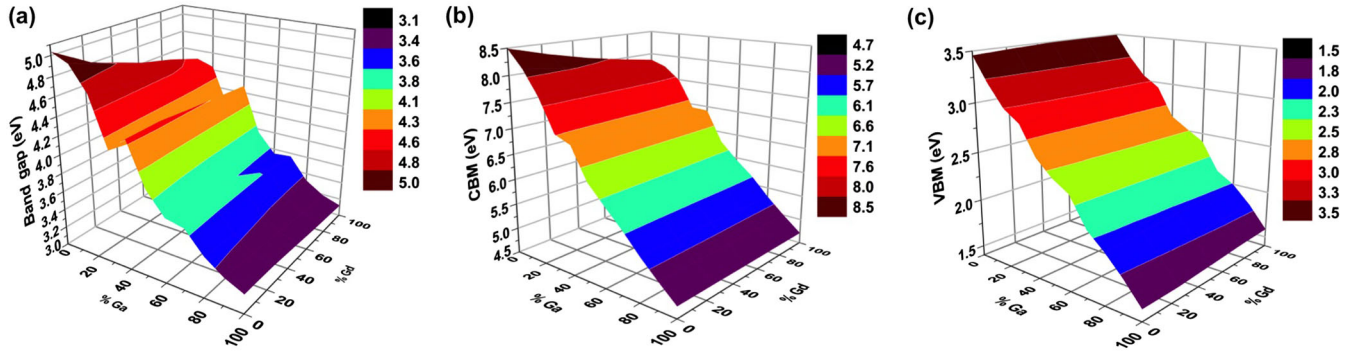

FIG. 7. Variation of (a) band gap (eV), (b) CBM (eV), and (c) VBM (eV) as a function of Gd (x) and Ga (y) concentration in $(Lu_{1-x}Gd_x)_3(Al_{1-y}Ga_y)_5O_{12}$.

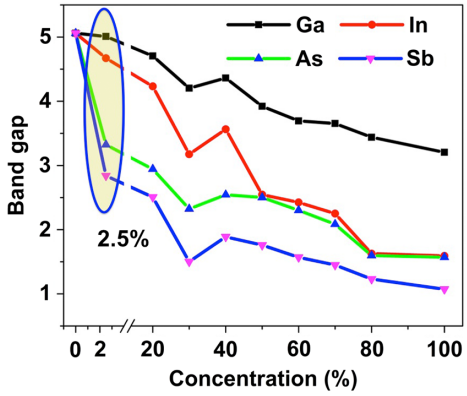

FIG. 8. Variation of the band gap (eV) as a function of B (where B is Ga, In, As, and Sb) concentration, substituting for Al in $Lu_3(Al_{1-x}B_x)_5O_{12}$. The smallest possible concentration in our simulation cells (2.5%) is highlighted by the circle.

that doping with a smaller concentration of In compared to Ga will have the same effect on the CBM. Also, the band-gap shift resulting from As and Sb doping is markedly different from Ga. Specifically, there are two regimes where the biggest shift in the band gap occurs at relatively low concentrations, and above 40% As or Sb, the band-gap shift is again linear and similar to Ga. That is, after an initial large shift in the band gaps induced by In or As, the subsequent changes are similar to those induced by Ga. The sharp initial drop in the band gap due to doping with either As or Sb can be interpreted as follows. With a small amount of dopant, a deep dopant level is created that forms the new valence-band edge. With increasing dopant concentration, the new valence band widens and, consequently, further reduces the band gap but only modestly compared to the initial drop. Further, the results in Fig. 8 suggest that band-gap changes induced by ionic species such as In and Ga are relatively linear, while those produced by more covalent materials exhibit a less linear but still monotonic dependence on admixed ion concentration.

IV. DISCUSSION

Our results suggest that both strain and chemistry play important roles in determining the band gap and the relative position of band edges in $A_3B_5O_{12}$ garnets. Cations with larger radii tend to produce smaller band gaps. This is accompanied by an increase in the lattice parameter. This suggests that the cation radius can be used as an initial screening parameter in the search for candidate dopants to modify the band gap. However, while we consider extreme limits of full substitution, some of these hypothetical compounds may not be realizable experimentally. This may explain the need to codope $Lu_3Al_5O_{12}$ with both Ga and Gd. Gd having a larger radius than Lu will help maintain the $A:B$ radius ratio in $A_3B_5O_{12}$ garnets, stabilizing the compound. Further, also as a consequence of the larger size, Gd will suppress excess antisite formation between the A and B sites, as it will increase the average disparity in cation size between the two sites.

It might also be advantageous to dope or admix with smaller amounts of larger cations. For example, the band-gap change for In-substituted LuAG is much larger than for Ga-substituted LuAG. One might be able to achieve the same shifts in the CBM exhibited for full substitution of Ga by relatively modest amounts of In substitution. This finding will provide more opportunities for admixing strategies, as we discuss below.

To better isolate the roles of strain and chemistry, we calculate the band gap of all of the compounds considered when they are strained to the lattice constant of $Lu_3Al_5O_{12}$. These results are shown in Figs. 3(b) and 6(b) with the line labeled strained. For both Al and Lu substitution, the band gaps for the compounds at their natural lattice constant and when strained to the $Lu_3Al_5O_{12}$ lattice constant show very similar behavior. This indicates that the changes in the band edges are not simply a consequence of strain induced by changing the radii of the cations, but, rather, it is an effect inherent in the chemistry of the cations. Thus, while the cation radius seems to correlate with the changes in the band gap, it is not a direct cause of those changes.

Our results suggest admixing strategies to finely tune the band edges of complex oxide compounds for applications such as scintillators. One can imagine admixing LuAG with both Ga and As, the first to lower the CBM and remove electron traps and the second to raise the VBM and eliminate hole traps. An implication of the nonlinear variation of band edges is that a very small amount of In, As, and Sb will have a much larger effect on band edges. Of course, the stability of such chemically complex garnets must be examined, but by choosing the appropriate dopant species and concentrations, the band edges, in principle, can be tuned to very precise values. In fact, the results in Fig. 3 suggest that if one were to codope with In and either As or Sb, the band gap might be eliminated altogether. If such a compound is not thermodynamically stable, there might be other dopants that can achieve the same effect. In addition, in multicomponent garnets, a positive effect on light yield is also expected due to local chemical composition fluctuation and related band-edge fluctuations which may limit the out-of-track migration of charge carriers, thus, supporting their immediate radiative recombination at emission centers [49].

Ce^{3+} is a typical dopant used as a center for photoluminescence. The upward shift of the VBM with admixing by As and Sb will reduce the energy gap between the VBM and the Ce^{3+} ground state, which might facilitate the hole transfer from the valence band towards the Ce^{3+} center in multicomponent garnet hosts. In YAG, LuAG, and GGAG, this energy gap is estimated to be about 3.6 eV [15]. Such a large energy gap can, indeed, lower the probability of fast hole transfer towards Ce^{3+}. An optimum gap value in this case is usually considered within 0.5–1 eV [50]. Thus, with

the right concentrations of As or Sb, this VBM Ce gap can be reduced to optimal values.

V. CONCLUSIONS

Admixing $R_3Al_5O_{12}$ garnet compounds with Ga and Gd leads to pronounced improvements in scintillator performance, in part due to shifts in the conduction band such that the energy level of shallow defects is no longer in the forbidden gap. In this work, we screen for additional admixing species using first-principles DFT focusing on the variation of band edges in order to potentially band-edge engineer next-generation garnet scintillators. We show that certain dopants can influence the VBM, the CBM, or both, which opens the door for further admixing strategies to optimize scintillator compounds. We show that substituting Al with Ga, In, As, and Sb in LuAG changes the band gap, and with ionic elements (Ga and In), tends to decrease the band gap by lowering the CBM. On the other hand, covalent elements (Sb and As) tend to decrease the band gap by pushing the VBM higher in energy. In contrast, substituting Lu with Gd, Dy, or Er changes neither the band gap nor the band edges to any significant degree. This study opens the possibility of tuning band gaps and band edges by admixing not only garnets but other complex oxides as well. The ability to control band gaps and band edges independently is a powerful tool to optimize the performance of various materials for technological applications including not only scintillation, but also solar cells, light-emitting diodes, and field-effect transistors that require proper alignment of band edges across heterostructures.

ACKNOWLEDGMENTS

B. P. U. is supported by the U.S. Department of Energy, Office of Science, Basic Energy Sciences, Materials Sciences and Engineering Division. M. N. acknowledges partial support of Czech National Science Foundation Grant No. P204/12/0805. C. R. S. and S. K. Y. gratefully acknowledge support of the Nonproliferation Research and Development Program within the U.S. National Nuclear Security Administration. The Los Alamos National Laboratory, an affirmative action equal opportunity employer, is operated by Los Alamos National Security, LLC, for the National Nuclear Security Administration of the U.S. Department of Energy under Contract No. DE-AC52-06NA25396.

[1] J. Geusic, H. Marcos, and L. Vanuitert, Laser oscillations in Nd-doped yttrium aluminum, yttrium gallium and gadolinium garnets, Appl. Phys. Lett. **4**, 182 (1964).

[2] G. Blasse and A. Bril, A new phosphor for flying-spot cathode-ray tubes for color television: Yellow-emitting $Y_3Al_5O_{12}$-Ce^{3+}, Appl. Phys. Lett. **11**, 53 (1967).

[3] M. Weber, Nonradiative decay from 5d states of rare earths in crystals, Solid State Commun. **12**, 741 (1973).

[4] M. Moszynski, T. Ludziejewski, D. Wolski, W. Klamra, and L. Norlin, Properties of the YAG: Ce scintillator, Nucl. Instrum. Methods Phys. Res., Sect. A **345**, 461 (1994).

[5] M. Weber, Scintillation: Mechanisms and new crystals, Nucl. Instrum. Methods Phys. Res., Sect. A **527**, 9 (2004).

[6] M. Nikl, E. Mihokova, J. Pejchal, A. Vedda, M. Fasoli, I. Fontana, V. Laguta, V. Babin, K. Nejezchleb, and A. Yoshikawa, Scintillator materials-achievements, opportunities, and puzzles, IEEE Trans Nucl. Sci. **55**, 1035 (2008).

[7] T. Kanai, M. Satoh, and I. Miura, Characteristics of a nonstoichiometric Gd^{3+} δ $(Al, Ga)_5$-δO_{12}: Ce garnet scintillator, J. Am. Ceram. Soc. **91**, 456 (2008).

[8] N. Cherepy, J. Kuntz, Z. Seeley, S. Fisher, O. Drury, B. Sturm, T. Hurst, R. Sanner, J. Roberts, and S. Payne, Transparent ceramic scintillators for gamma spectroscopy and radiography, SPIE Int. Soc. Opt. Eng. **7805**, 78050I (2010).

[9] K. Kamada, T. Yanagida, J. Pejchal, M. Nikl, T. Endo, K. Tsutumi, Y. Fujimoto, A. Fukabori, and A. Yoshikawa, Scintillator-oriented combinatorial search in Ce-doped $(Y, Gd)_3(Ga, Al)_5O_12$ multicomponent garnet compounds, J. Phys. D **44**, 505104 (2011).

[10] K. Kamada, T. Endo, K. Tsutumi, T. Yanagida, Y. Fujimoto, A. Fukabori, A. Yoshikawa, J. Pejchal, and M. Nikl, Composition engineering in cerium-doped $(Lu, Gd)_3(Ga, Al)_5O_{12}$ single-crystal scintillators, Cryst. Growth Design **11**, 4484 (2011).

[11] M. Nikl, A. Yoshikawa, K. Kamada, K. Nejezchleb, C. R. Stanek, J. Mares, and K. Blazek, Development of LuAG-based scintillator crystals-A review, Progr. Cryst. Growth Charact. Mater. **59**, 47 (2013).

[12] M. Tyagi, F. Meng, M. Koschan, S. B. Donnald, H. Rothfuss, and C. L. Melcher, Effect of codoping on scintillation and optical properties of a Ce-doped $Gd_3Ga_3Al_2O_{12}$ scintillator, J. Phys. D **46**, 475302 (2013).

[13] J. M. Ogiegło, A. Katelnikovas, A. Zych, T. Jstel, A. Meijerink, and C. R. Ronda, Luminescence and luminescence quenching in $Gd_3(Ga, Al)_5O_{12}$ scintillators doped with Ce^{3+}, J. Phys. Chem. A **117**, 2479 (2013).

[14] W. Drozdowski, K. Brylew, M. Witkowski, A. Wojtowicz, P. Solarz, K. Kamada, and A. Yoshikawa, Studies of light yield as a function of temperature and low temperature thermoluminescence of $Gd_3Al_2Ga_3O_{12}$: Ce scintillator crystals, Opt. Mater. **36**, 1665 (2014).

[15] Y. Wu, F. Meng, Q. Li, M. Koschan, and C. L. Melcher, Role of Ce^{4+} in the Scintillation Mechanism of Codoped $Gd_3Ga_3Al_2O_{12}$: Ce, Phys. Rev. Applied **2**, 044009 (2014).

[16] P. Sibczynski, J. Iwanowska-Hanke, M. Moszynski, L. Swiderski, M. Szawlowski, M. Grodzicka, T. Szczesniak, K. Kamada, and A. Yoshikawa, Characterization of GAGG: Ce scintillators with various Al-to-Ga ratio, Nucl. Instrum. Methods Phys. Res., Sect. A **772**, 112 (2015).

[17] M. Nikl, A. Yoshikawa, K. Kamada, K. Nejezchleb, C. R. Stanek, J. Mares, and K. Blazek, Development of LuAG-based scintillator crystals—A review, Prog. Cryst. Growth Charact. Mater. **59**, 47 (2013).

[18] V. Lupei, A. Lupei, C. Tiseanu, S. Georgescu, C. Stoicescu, and P. M. Nanau, High-resolution optical spectroscopy of YAG: Nd: A test for structural and distribution models, Phys. Rev. B **51**, 8 (1995).

[19] M. Nikl, E. Mihokova, J. Pejchal, A. Vedda, Y. Zorenko, and K. Nejezchleb, The antisite LuAl defect-related trap in $Lu_3Al_5O_{12}$: Ce single crystal, Phys. Status Solidi B **242**, R119 (2005).

[20] H. Donnerberg and C. Catlow, Atomistic computer simulations of yttrium iron garnet (YIG) as an approach to materials defect chemistry. I. Intrinsic defects, J. Phys. Condens. Matter **5**, 2947 (1993).

[21] M. M. Kuklja, Defects in yttrium aluminium perovskite and garnet crystals: Atomistic study, J. Phys. Condens. Matter **12**, 2953 (2000).

[22] C. Milanese, V. Buscaglia, F. Maglia, and U. Anselmi-Tamburini, Disorder and nonstoichiometry in synthetic garnets $A_3B_5O_{12}$ (A = Y, Lu-La, B = Al, Fe, Ga). A simulation study, Chem. Mater. **16**, 1232 (2004).

[23] C. R. Stanek, K. McClellan, M. Levy, C. Milanese, and R. Grimes, The effect of intrinsic defects on $RE_3Al_5O_{12}$ garnet scintillator performance, Nucl. Instrum. Methods Phys. Res., Sect. A **579**, 27 (2007).

[24] M. Nikl, The antisite LuAl defect-related trap in $Lu_3Al_5O_{12}$: Ce single crystal, Phys. Status Solidi (a) **202**, 201 (2005).

[25] M. Nikl, J. Pejchal, E. Mihokova, J. Mares, H. Ogino, A. Yoshikawa, T. Fukuda, A. Vedda, and C. D'Ambrosio, Antisite defect-free $Lu_3(Ga_xAl_{1-x})_5O_{12}$: Pr scintillator, Appl. Phys. Lett. **88**, 141916 (2006).

[26] R. Shannon, Revised effective ionic radii and systematic studies of interatomic distances in halides and chalcogenides, Acta Crystallogr., Sect. A **32**, 751 (1976).

[27] G. Shirinyan, K. Ovanesyan, A. Eganyan, A. Petrosyan, C. Pedrini, C. Dujardin, I. Kamenskikh, and N. Guerrassimova, X-ray and optical studies of ytterbium-doped gallium garnets, Nucl. Instrum. Methods Phys. Res., Sect. A **537**, 134 (2005).

[28] C. R. Stanek, C. Jiang, S. K. Yadav, K. McClellan, B. P. Uberuaga, D. A. Andersson, and M. Nikl, The effect of Ga-doping on the defect chemistry of $RE_3Al_5O_{12}$ garnets, Phys. Status Solidi B **250**, 244 (2013).

[29] M. Fasoli, A. Vedda, M. Nikl, C. Jiang, B. P. Uberuaga, D. A. Andersson, K. J. McClellan, and C. R. Stanek, Band-gap engineering for removing shallow traps in rare-earth $Lu_3Al_5O_{12}$ garnet scintillators using Ga^{3+} doping, Phys. Rev. B **84**, 081102(R) (2011).

[30] G. Kresse and J. Furthmüller, Efficient iterative schemes for *ab initio* total-energy calculations using a plane-wave basis set, Phys. Rev. B **54**, 11169 (1996).

[31] J. P. Perdew, K. Burke, and M. Ernzerhof, Generalized Gradient Approximation Made Simple, Phys. Rev. Lett. **77**, 3865 (1996).

[32] P. E. Blöchl, Projector augmented-wave method, Phys. Rev. B **50**, 17953 (1994).

[33] A. V. Krukau, O. A. Vydrov, A. F. Izmaylov, and G. E. Scuseria, Influence of the exchange screening parameter on the performance of screened hybrid functionals, J. Chem. Phys. **125**, 224106 (2006).

[34] S.-H. Wei and A. Zunger, Band offsets and optical bowings of chalcopyrites and Zn-based II-VI alloys, J. Appl. Phys. **78**, 3846 (1995).

[35] P. G. Moses and C. G. Van de Walle, Band bowing and band alignment in InGaN alloys, Appl. Phys. Lett. **96**, 021908 (2010).

[36] C. G. Van de Walle and R. M. Martin, Theoretical calculations of heterojunction discontinuities in the Si/Ge system, Phys. Rev. B **34**, 5621 (1986).

[37] A. Franciosi and C. G. Van de Walle, Heterojunction band offset engineering, Surf. Sci. Rep. **25**, 1 (1996).

[38] V. Venkatramu, M. Giarola, G. Mariotto, S. Enzo, S. Polizzi, C. Jayasankar, F. Piccinelli, M. Bettinelli, and A. Speghini, Nanocrystalline lanthanide-doped $Lu_3Ga_5O_{12}$ garnets: Interesting materials for light-emitting devices, Nanotechnology **21**, 175703 (2010).

[39] X. Xu, J. Chen, S. Deng, N. Xu, and J. Lin, Cathodoluminescent properties of nanocrystalline $Lu_3Ga_5O_{12}$: Tb^{3+} phosphor for field emission display application, J. Vac. Sci. Technol. B **28**, 490 (2010).

[40] V. Mahalingam, F. Mangiarini, F. Vetrone, V. Venkatramu, M. Bettinelli, A. Speghini, and J. A. Capobianco, Bright white upconversion emission from $Tm^{3+}/Yb^{3+}/Er^{3+}$-doped $Lu_3Ga_5O_{12}$ nanocrystals, J. Phys. Chem. C **112**, 17745 (2008).

[41] A. Raevsky, A. Gukalova, and G. Semin, Nuclear quadrupole resonance of antimony in $Ln_3Sb_5O_{12}$ crystals, Z. Naturforsch. A **49**, 687 (1994).

[42] Y. Zorenko, V. Gorbenko, I. Konstankevych, A. Voloshinovskii, G. Stryganyuk, V. Mikhailin, V. Kolobanov, and D. Spassky, Single-crystalline films of Ce-doped YAG and LuAG phosphors: Advantages over bulk crystals analogues, J. Lumin. **114**, 85 (2005).

[43] S. K. Yadav and R. Ramprasad, Appl. Phys. Lett. **100**, 241903 (2012).

[44] S. K. Yadav, V. Sharma, and R. Ramprasad, Controlling electronic structure through epitaxial strain in ZnSe/ZnTe nano-heterostructures, J. Appl. Phys. **118**, 015701 (2015).

[45] K. Yang, Y. Dai, and B. Huang, J. Phys. Chem. C **111**, 18985 (2007).

[46] R. F. Bader, *Atoms in Molecules* (Wiley Online Library, New York, 1990).

[47] W. Tang, E. Sanville, and G. Henkelman, A grid-based Bader analysis algorithm without lattice bias, J. Phys. Condens. Matter **21**, 084204 (2009).

[48] A. Zunger, S.-H. Wei, L. G. Ferreira, and J. E. Bernard, Special Quasirandom Structures, Phys. Rev. Lett. **65**, 353 (1990).

[49] A. V. Gektin, A. N. Belsky, and A. N. Vasil'ev, Scintillation efficiency improvement by mixed crystal use, IEEE Trans. Nucl. Sci. **61**, 262 (2014).

[50] P. Dorenbos, Fundamental limitations in the performance of Ce^{3+}, Pr^{3+} and—Eu^{2+} activated scintillators, IEEE Trans. Nucl. Sci. **57**, 1162 (2010).